Journal Homepage: -www.journalijar.com

INTERNATIONAL JOURNAL OF ADVANCED RESEARCH (IJAR)

Article DOI:10.21474/IJAR01/23962
DOI URL: http://dx.doi.org/10.21474/IJAR01/23962

RESEARCH ARTICLE

ZINC OXIDE (ZnO) THIN FILMS SYNTHESIZED VIA COMBINED SPIN COATING AND CHEMICAL BATH DEPOSITION METHODS: THE INFLUENCE OF PRECURSOR CONCENTRATION ON THE PHYSICAL PROPERTIES

M. Baneto[1,2], M. Badjemna[1,2], O. Ako[1,2], A. D. Gboglo[1,2], A.R. Ali-Tagba[1,2], M. Kouide[1,2], D. Djagbai[1,2] and J. S. Aklamanu[1,2]

1. Centre d'ExcellenceRégional pour la Maîtrise de l'Electricité (CERME), University of Lomé, 01BP 1515, Lomé, Togo.
2. Laboratory on Solar Energy, Department of Physics, Faculty of Sciences, University of Lomé, 01BP 1515, Lomé, Togo.

Manuscript Info

Manuscript History
Received: 10 June 2026
Final Accepted: 12 July 2026
Published: August 2026

Key words:-
Thin films;Zinc Oxide; Chemical bath deposition;Physical properties.

Abstract

In this study, zinc oxide (ZnO) thin films were elaborated via a two-step process. The first step consisted of depositing a ZnO seed layer onto microscopic glass slide substrates using the spin-coating technique, with zinc acetate dihydrate as the precursor and ethanol as the solvent, at a precursor concentration of 0.01 M. The second step involved the growth of ZnO thin films by chemical bath deposition on the pre-seeded substrates, with the precursor concentration varied from 0.05 M to 0.30 M in increments of 0.05 M. The resulting thin films were subsequently annealed at 400 °C for 3 hours. The effect of precursor concentration on the structural and optical properties of the ZnO thin films was investigated using X-ray diffraction (XRD), UV-visible spectroscopy, and photoluminescence (PL) spectroscopy. The characterization results clearly reveal the significant influence of precursor concentration on the physical properties of the ZnO thin films.XRD analysis indicates that all synthesized films are polycrystalli ne and crystallize in a hexagonal wurtzite structure, exhibiting a preferential orientation along the (002) plane with increasing precursor concentration. UV-visible spectroscopy results show that all ZnO thin films are highly transparent, with transmittance exceeding 80 %. The optical band gap of the prepared films ranges from 3.18 eV to 3.25 eV. Photoluminescence spectra exhibit three emission peaks centered at approximately 390 nm (3.18 eV), 446 nm (2.78 eV), and 490 nm (2.53 eV). The dominant peak at 390 nm is attributed to free exciton recombination, corresponding to the direct band-to-band transition.

The blue emissions observed at 446 nm (2.78 eV) and 490 nm (2.53 eV) in the visible region are associated with intrinsic defects in ZnO.

Corresponding Author:-M. Baneto
Address:-1.Centre d'Excellence Régional pour la Maîtrise de l'Electricité(CERME), University of Lomé, 01BP 1515, Lomé, Togo.2. Laboratory on Solar Energy, Department of Physics, Faculty of Sciences, University of Lomé, 01BP 1515, Lomé, Togo.

Introduction:-

Zinc oxide (ZnO) is an n-type semiconductor material distinguished by several remarkable properties. It's exhibits a wide direct band gap (3.37 eV), a high exciton binding energy (60 meV) [1] , excellent chemical and thermal stability[2], efficient room-temperature emission [3], non-toxicity, and high transparency in the visible region [3]. Furthermore, the diversity of its synthesis routes and its intrinsic piezoelectric nature make ZnO a particularly attractive material for various technological applications [4]. Owing to these properties, ZnO thin films have found extensive applications in the field of optoelectronics. They are widely employed in light-emitting diodes (LEDs) [5], lasers, piezoelectric nanogenerators [6], transistors [7], gas sensors [8], photocatalysis [9], and solar cells [10]. Various techniques have been reported for the synthesis of ZnO thin films, including both physical and chemical approaches. Physical methods such as thermal evaporation [11], sputtering [12], pulsed laser deposition (PLD) [13], and molecular beam epitaxy (MBE) [14] are commonly used. However, these techniques are generally complex and require expensive vacuum-based equipment. In contrast, chemical methods offer a simpler and more cost-effective alternative for the fabrication of ZnO thin films.

These include chemical vapor deposition (CVD) [15], hydrothermal synthesis [16], spray pyrolysis [17], electrodeposition [18], sol-gel methods (dip-coating or spin-coating) [19,20]and chemical bath deposition (CBD) [21,22]. Among these, CBD has emerged as a particularly attractive technique for thin film growth due to its numerous advantages, such as low processing temperature, ease of implementation, low cost, good reproducibility, and environmentally friendly nature [23,24]. Despite these advantages, CBD presents some limitations, particularly the difficulty in precisely controlling the size, morphology, and orientation of ZnO nanostructures [25]. To overcome these challenges, a two-step approach is often adopted, involving the prior deposition of a ZnO seed layer (via spin-coating or spray pyrolysis), followed by a CBD growth process [22,25]. It is well established that the final properties of ZnO nanostructures strongly depend on growth conditions such as chemicals molar ratio[26],precursor concentration [27], substrate position in the bath [28], temperature [24], solution pH [29], and growth time [21]. Among these parameters, precursor concentration plays a crucial role in tailoring ZnO nanostructures with enhanced physical properties [27]. Several studies have investigated the influence of precursor concentration on the properties of ZnO thin films synthesized using a combination of sol-gel and chemical bath deposition (CBD) techniques [10,30,31]. However, in most reported works, the substrates are generally placed vertically in the growth solution during the CBD process. In the present study, a different approach was adopted by using a horizontal substrate configuration in the chemical bath.

In this work, the effect of precursor concentration on the structural and optical properties of ZnO thin films prepared through a two-step process was investigated. The first step consisted of depositing a ZnO seed layer on microscopic glass slide substrates using the spin-coating technique. The second step involved the growth of ZnO nanostructures by chemical bath deposition (CBD) on the substrates previously coated with the ZnO seed layer. The precursor concentration was varied from 0.05 M to 0.30 M with a step of 0.05 M.

Materials and Methods:-

Materials and Reagents:-

In this study, microscopic glass slides were used as substrates. Zinc acetate dihydrate and zinc nitrate hexahydrate were employed as precursor sources. Hexamethylenetetramine (HMTA) was used as a complexing agent. Ethanol (C_2H_6O), acetone [$(CH_3)_2CO$], and distilled water served as solvents. All chemicals were supplied by Thermo and Fisher Scientifics with a purity higher than 99 % and were used without any further purification. A HOLMARC spin coater and a hot plate were used for the deposition of the ZnO seed layer and the pre-annealing process, respectively. A custom-built setup was designed in the laboratory for the chemical bath deposition (CBD) growth. The overall growth process consisted of two main steps.

Substrate Cleaning:-

The glass slides were cut into 2.5 cm × 2.5 cm samples using a substrate cutter, making them suitable for the experimental deposition conditions. Prior to seed layer deposition, the substrates were thoroughly cleaned to improve film adhesion, ensure uniform thickness distribution, and preserve the functional properties of the seed layer. The cleaning procedure began with a single ultrasonic washing step in soapy water for 15 minutes. This was followed by sequential ultrasonic cleaning in distilled water, acetone, ethanol, and finally distilled water again, with each step lasting 15 minutes. After the cleaning process, the substrates were dried using a hot-air dryer before seed layer deposition.

Seed Layers Deposition by Spin Coating:-

ZnO seed layers were deposited on the pre-cleaned glass substrates using the spin-coating technique, with zinc acetate dihydrate as the precursor and ethanol as the solvent. A 10 mM solution was prepared by dissolving 0.044 g of zinc acetate dihydrate in 20 mL of ethanol. The solution was stirred using a magnetic stirrer for 20 minutes at room temperature until a clear and homogeneous solution was obtained. The resulting solution was then used for the deposition of the ZnO seed layer by spin coating, with a deposition time of 45 s and a rotation speed of 1500 rpm. The deposited seed layers were subsequently pre-annealed at 150 °C for 2 minutes on a hot plate to evaporate the solvent and remove organic residues. The spin-coating and pre-annealing processes were repeated 10 times to ensure a uniform coating of ZnO seed particles on the substrate. The formation of ZnO nanocrystals on the substrate provided a nucleation layer for the subsequent growth of ZnO nanostructures. The deposition process is summarized in Figure 1.

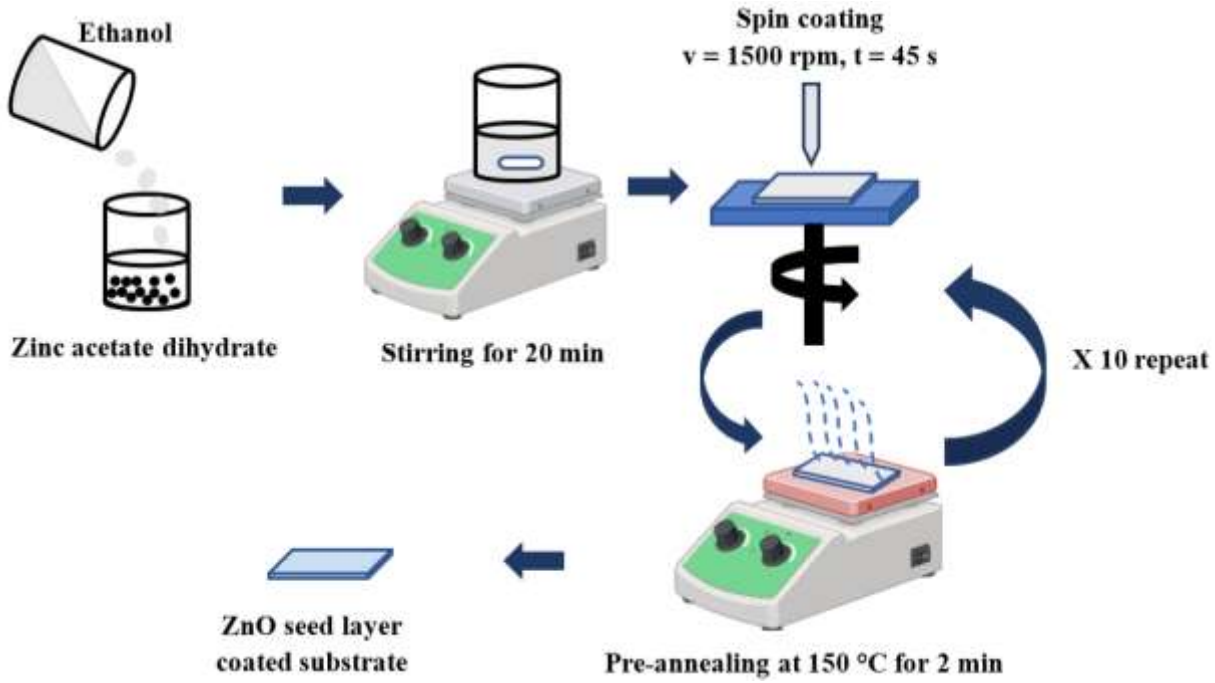

Figure 1: Schematic illustration of the ZnO seed layer deposition process.

Chemical Bath Deposition (CBD) Growth:-

ZnO thin films were synthesized via chemical bath deposition (CBD) on previously deposited seed layers. Zinc nitrate hexahydrate ($Zn(NO_3)_2 \cdot 6H_2O$) and hexamethylenetetramine ($C_6H_{12}N_4$)were used as the precursor and complexing agent, respectively, while distilled water served as the solvent. To investigate the effect of precursor concentration on the physical properties of the nanostructures, six samples were prepared by varying the concentration from 0.05 M to 0.30 M in increments of 0.05 M. The growth solution was prepared by mixing equimolar aqueous solutions of zinc nitrate hexahydrate and HMTA. Specifically, 50 mL of zinc nitrate hexahydrate solution and 50 mL of HMTA solution were prepared separately and then combined to obtain a single 100 mL growth solution. The resulting solution was stirred using a magnetic stirrer until a perfectly homogeneous mixture was achieved. To prevent deposition on both sides of the substrate, two substrates were stacked together: one bearing the ZnO seed layer and another plain glass substrate acting as a protective cover for the opposite face. This assembly was then placed on a substrate holder and immersed horizontally in the growth solution, ensuring that it did not come into contact with the bottom of the beaker. The temperature of the solution was maintained at a constant 80 °C using a heating bath. Continuous stirring was applied throughout the growth process using a magnetic stirrer. The growth duration was fixed at 1 hour. A mercury thermometer was used to monitor the bath temperature, while a stopwatch was employed to measure the deposition time. At the end of the growth process, the samples were removed from the bath and dried at room temperature. All synthesized samples were subsequently annealed at 400 °C in a Nabertherm furnace for 3 hours to improve the crystallinity of the ZnO thin films[32].The overall growth process is summarized in Figure 2.

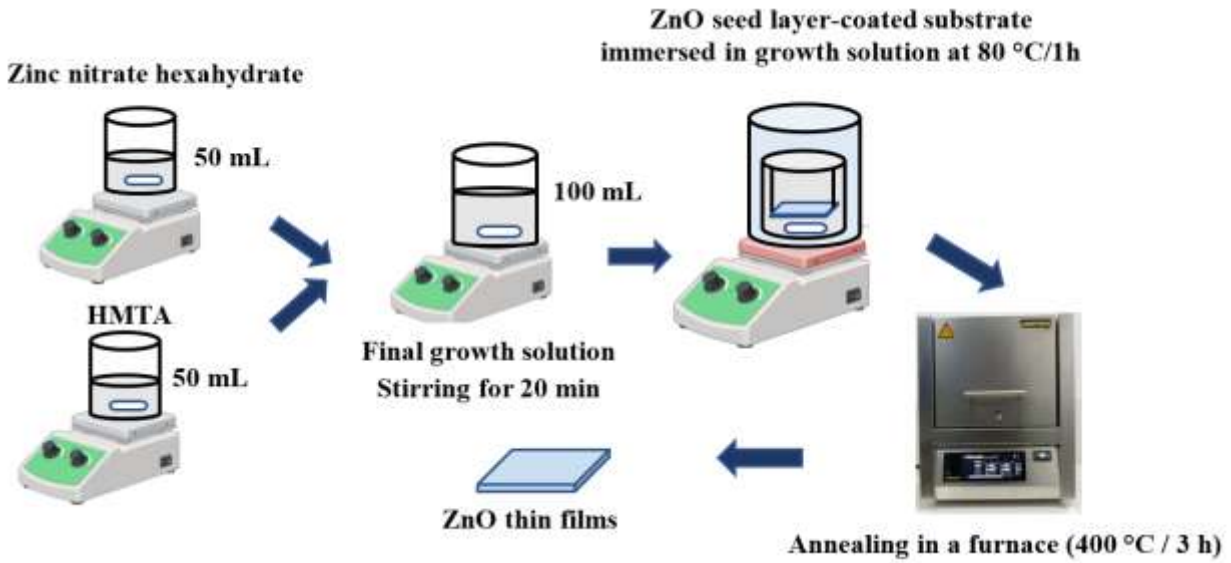

Figure 2: Schematic illustration of the ZnO thin films deposition process by chemical bath deposition (CBD).

ZnO Thin Films Characterization:-

To investigate the properties of the synthesized thin films, several characterization techniques were employed. The crystalline structure of the ZnO thin films was determined using an X-ray diffractometer (Empyrean model) equipped with a CuKα radiation source (λ = 1.54059 Å). The optical properties of ZnO thin films were measured using a UV-visible spectrophotometer (Lambda 800 model). Electronic transitions and defect-related emissions were analyzed using a photoluminescence spectrometer (Ocean Optics model) equipped with a diode laser as the excitation source at a wavelength of 405 nm.

Results and Discussion:-

Structural Properties:-

Figure 3 shows the X-ray diffraction (XRD) patterns of ZnO thin films synthesized with varying zinc nitrate precursor concentrations ranging from 0.05 M to 0.30 M, in steps of 0.05 M. The diffraction patterns exhibit three peaks located at 2θ values of 31.69°, 34.73°, and 36.62°, which are indexed to the (100), (002), and (101) crystallographic planes, respectively. All identified diffraction peaks correspond to the hexagonal wurtzite structure of ZnO with the space group $P6_3mc$, in agreement with the standard JCPDS card No. 36-1451 [33].All ZnO thin films are polycrystalline, and no peaks related to secondary phases were detected, indicating the high purity of the synthesized films [34]. The XRD patterns clearly reveal the influence of precursor concentration on the crystallinity of the prepared thin films. At a concentration of 0.05 M, the diffraction peaks exhibit very low intensity, which can be attributed to weak nucleation resulting from insufficient precursor concentration [35]. This limits the availability of Zn^{2+} and OH^- ions required for ZnO formation. Therefore, Zn^{2+} and OH^- ions play a crucial role in the growth mechanism, and the zinc precursor concentration directly affects the growth behavior and properties of ZnO thin films [34]. As the precursor concentration increases, a decrease in the intensity of the (100) and (101) peaks and a significant enhancement of the (002) peak intensity is observed, indicating a preferential growth along the c-axis. Thus, increasing the precursor concentration promotes higher nucleation density and favors oriented growth along the (002) plane, leading to a perpendicular alignment of ZnO crystallites with respect to the substrate [36]. These findings are in good agreement with previously reported results in the literature [34–37]. To further confirm the degree of preferential orientation of the crystallites along the (002) plane, the texture coefficient $T_{c(hkl)}$ for each diffraction peak was calculated using Equation (1)[40] and the corresponding values are presented in Table 1.

$$T_{c(hkl)} = \frac{\left[\frac{I_{(hkl)}}{I_{r(hkl)}}\right]}{\left[\frac{1}{n}\sum\left(\frac{I_{(hkl)}}{I_{r(hkl)}}\right)\right]} \quad (1)$$

where $T_{c(hkl)}$ is the texture coefficient, $I_{(hkl)}$ represent the X-ray diffraction (XRD) intensities obtained from the thin films, and n is the number of diffraction peaks considered, $I_{r(hkl)}$ denotes the standard reference XRD intensity (JCPDS card No. 36-1451), corresponding to randomly oriented crystallites.

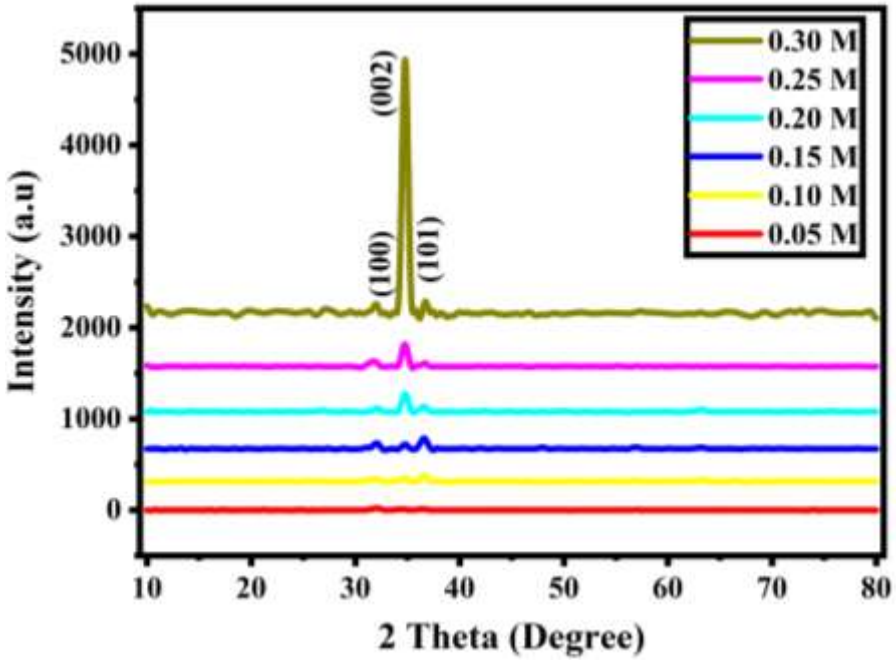

Figure 3: XRD spectra of ZnO thin films prepared at different precursor concentrations.

Table 1: Texture coefficient of ZnO thin films along (100), (002) and (101) plan at different precursor concentrations.

Concentration (M)	$T_{C(hkl)}$		
	(100)	(002)	(101)
0.05	1.461	1.111	0.428
0.10	1.131	1.254	0.614
0.15	1.104	1.294	0.602
0.20	0.827	1.656	0.517
0.25	0.381	2.307	0.311
0.30	0.121	2.764	0.115

The texture coefficient along the (002) plane is greater than unity and increases with increasing precursor concentration, confirming the preferential growth along the (002) orientation. In contrast, the intensities of the (100) and (101) peaks decrease as the precursor concentration increases. The calculated $T_{c(hkl)}$ values for each sample are in good agreement with the XRD patterns. The enhancement of the (002) peak intensity with increasing concentration has also been reported by Ako et al. [37] and Abuelsamen et al. [34]. The lattice parameters a and c, as well as the interplanar spacing $d_{(hkl)}$ of the synthesized ZnO thin films, were determined using Bragg's law according to Equations (2) and (3) [41], and the results are presented in Table 2.

$$a = \frac{\lambda}{\sqrt{3}\sin\theta} \text{ and } c = \frac{\lambda}{\sin\theta} \quad (2)$$

$$d_{(hkl)} = \frac{\lambda}{2\sin\theta} \quad (3)$$

where λ represents the CuKα wavelength (1.54059 Å), and θ is the diffraction angle corresponding to the peak position. It is observed that the lattice parameters a and c of the samples synthesized at different precursor concentrations are in close agreement with those reported in the JCPDS card No. 36-1451 for zinc oxide [33].

Table 1. Lattice parameters and structural properties of ZnO thin films obtained along the (002) plane at different precursor concentrations.

Precursor concentration (M)	2θ (°)	β (°)	D(nm)	$d_{(hkl)}$ (Å)	δ ($\times 10^{15}$ligne/m^2)	Lattice parameters			ε (10^{-4})	V(Å^3)	L(Å)
						a (Å)	c (Å)	c/a			
0.05	34.394	1.012	7.499	2.605	17.782	3.227	5.211	1.615	13.666	46.997	1.969
0.10	34.688	0.716	10.593	2.584	8.912	3.262	5.168	1.584	9.555	47.610	1.978
0.15	34.757	0.559	13.558	2.579	5.440	3.227	5.158	1.598	7.637	46.528	1.963
0.20	34.731	0.654	11.588	2.581	7.447	3.242	5.162	1.592	8.928	46.983	1.969
0.25	34.730	0.628	12.072	2.581	6.862	3.257	5.162	1.585	8.570	47.432	1.976
0.30	34.752	0.617	12.279	2.579	6.633	3.239	5.159	1.593	8.431	46.862	1.967
JCPDS N° 31-1451	34.422	-	-	2.603	-	3.250	5.207	1.602	-	47.622	-

The calculated c/a ratio is also close to the standard value (1.602), suggesting that the obtained ZnO thin films exhibit a hexagonal close-packed structure [37]. The interplanar spacing values corresponding to the (002) plane is also found to be close to those of the JCPDS card No. 36-1451 [33]. In general, only slight variations in the interplanar spacing are observed with increasing precursor concentration.The crystallite size D of the different samples was calculated using the Debye-Scherrer formula (Equation (4)) [42].

$$D = \frac{k\lambda}{\beta\cos\theta} \quad (4)$$

where k is a shape factor with a typical value of 0.9, θ is the Bragg diffraction angle, λ (1.54059 Å) is the wavelength of the X-rays used, and β corresponds to the full width at half maximum (FWHM) of the diffraction peak, expressed in radians. The crystallite size of the samples prepared at different precursor concentrations is presented in Table 2. The crystallite size varies between 7.499 nm and 13.558 nm. At a concentration of 0.05 M, a small crystallite size (7.499 nm) is observed, which can be attributed to the low availability of Zn^{2+} and OH^- species. This reduces nucleation and crystal growth rates, leading to the formation of small crystallites and low crystallinity.When the concentration increases from 0.10 M to 0.15 M, an increase in crystallite size is observed, from 10.593 nm to 13.558 nm. This is due to improved crystallinity and enhanced, more homogeneous nucleation. At a concentration of 0.20 M, a slight decrease in crystallite size (11.588 nm) is observed, which may be attributed to a rapid growth process [43]. At higher concentrations (0.25 M and 0.30 M), the crystallite size tends to stabilize at approximately 12.279 nm.Although the film thickness was not directly measured in the present study, variations in precursor concentration are expected to affect the amount of deposited material and consequently the film thickness. Therefore, the observed changes in XRD peak intensities may arise not only from differences in crystallinity and preferred orientation, but also from possible variations in film thickness.The dislocation density (δ), which represents crystal lattice imperfections (defects), is estimated using Equation (5)[44].

$$\delta = \frac{1}{D^2} \quad (5)$$

The obtained values are presented in Table 2. A variation of the dislocation density with precursor concentration is observed, highlighting the influence of concentration on the crystalline quality of ZnO thin films. The dislocation density decreases significantly as the precursor concentration increases from 0.05 M to 0.15 M, indicating a progressive improvement in the crystalline quality of the ZnO thin films. This decrease is attributed to the increase in crystallite size. The reduction of dislocation density with increasing precursor concentration has been previously reported [45]. Beyond 0.05 M, a slight increase followed by a stabilization of the dislocation density is observed, which is associated with a minor reduction in crystallite size. The sample prepared at 0.05 M exhibits the highest dislocation density (17.782×10^{15} lines/m²), which may explain the relatively poor crystalline quality observed in the X-ray diffraction pattern for this concentration.The strain induced in powders due to crystal imperfection and distortion was calculated using the formula (6) [46].

$$\varepsilon = \frac{\beta}{4\tan\theta} \quad (6)$$

The corresponding values are presented in Table 2. The positive sign of the calculated strain indicates that the films are under tensile stress, reflecting an expansion of the crystal lattice compared to bulk ZnO. This strain is generally attributed to thermal mismatch between the thin film and the substrate, as well as to intrinsic stresses generated

during the deposition process [27,47,48]. The observed variations with precursor concentration reflect the balance between structural relaxation and internal stress effects.

The unit cell volume V of the hexagonal wurtzite structure and the Zn-O bond length L were calculated using Equations (7) and (8), respectively [49].

$$V = (\frac{\sqrt{3}}{2})a^2c \tag{7}$$

$$L = \sqrt{\frac{a^2}{3} + (\frac{1}{2} - u)^2c^2} \tag{8}$$

where u is a positional parameter in the wurtzite structure, representing the relative displacement of each atom along the c-axis with respect to the next one. It is expressed by the formula given in Equation (9)[50].

$$u = \frac{a^2}{3c^2} + 0.25 \tag{9}$$

The values of the unit cell volume and bond length have been summarized in Table 2. A slight variation in the unit cell volume is observed, while the bond length (L) remains nearly constant with increasing precursor concentration. This variation in volume results from changes in the 2θ angle of the (002) plane, since the unit cell volume is closely related to the lattice parameters a and c, which themselves vary with 2θ [27].

Optical Properties:-

Figure 4 shows the UV-Visible transmittance spectra of ZnO thin films synthesized with precursor concentrations ranging from 0.05 M to 0.30 M in steps of 0.05 M.

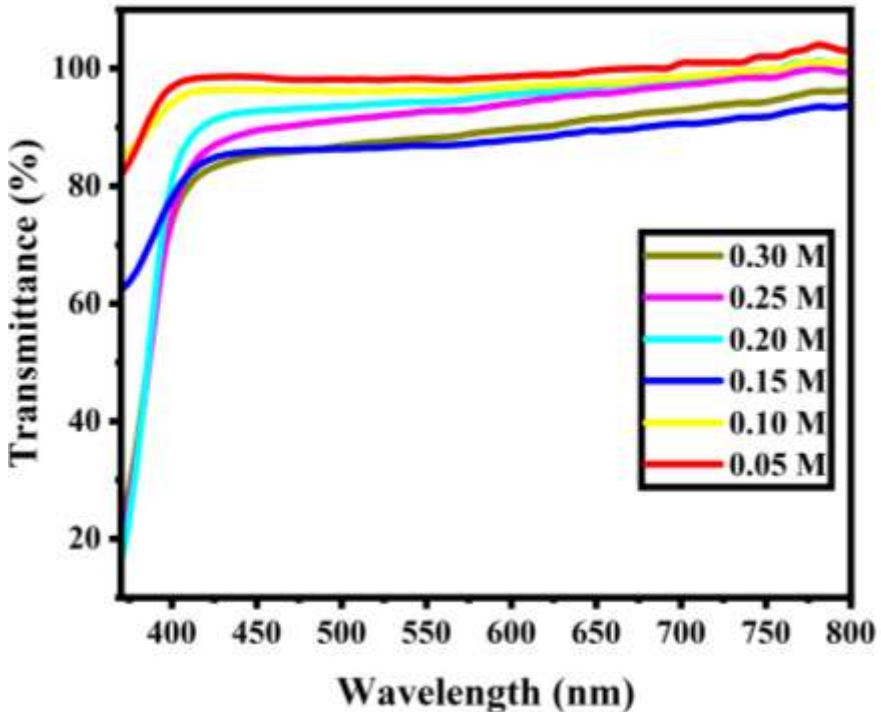

Figure 4: Transmittance spectra of ZnO thin films prepared at different precursor concentrations.

All ZnO thin films exhibit high transparency, with transmittance values exceeding 80 % in the visible region (400 - 800 nm). The transmittance spectra reveal fluctuations with increasing precursor concentration. A shift of the absorption edge toward the ultraviolet region is observed for samples prepared at 0.05 M, 0.10 M, and 0.15 M, along with transmittance values approaching 100 % (a characteristic of glass) in the visible region for the 0.05 M and 0.10 M samples. These observations can be explained by the low amount of deposited material at low precursor concentrations, leading to the formation of thin films with reduced thickness [51]. The decrease in film thickness

promotes a shift of the absorption edge and enhances light transmission in the visible range [52]. This results in higher transmittance values, close to that of the glass substrate, whose contribution becomes significant in the overall optical response of the thin film/substrate system.

Figure 5 illustrates the UV-Visible absorption spectra of ZnO thin films obtained at various precursor concentrations. A strong absorption is observed in the ultraviolet region, while the absorption remains low in the visible range, which is consistent with the high transparency of the films. These results are characteristic of ZnO [53].

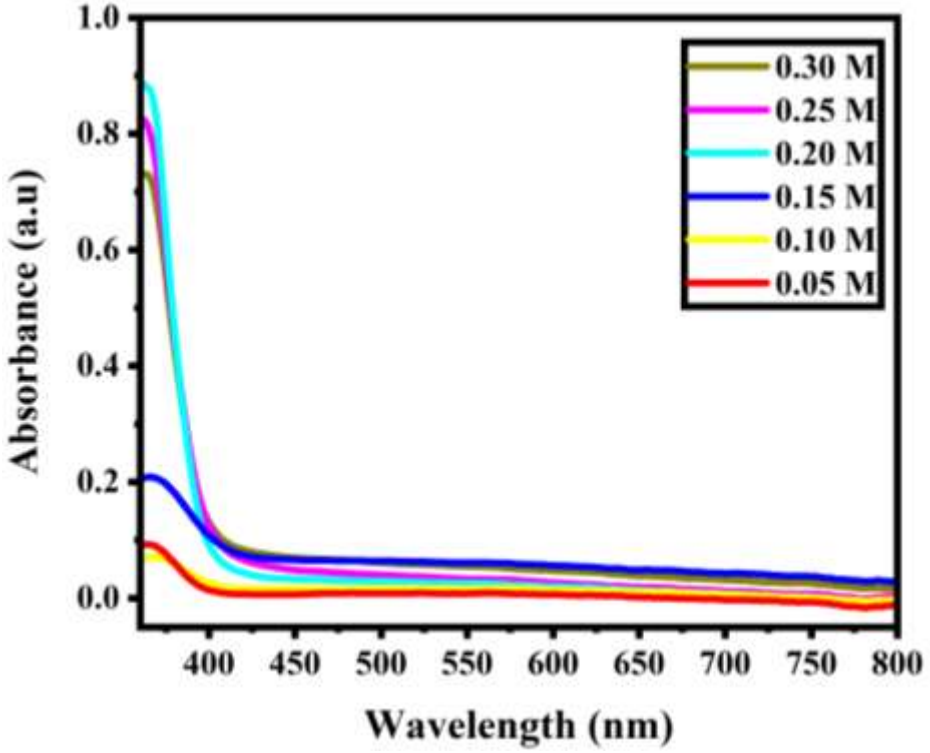

Figure 5: Absorbance spectra of ZnO thin films prepared at different precursor concentrations.

The optical band gap (E_g) values of the ZnO thin films were determined using the first derivative method. The derivative of the transmittance with respect to wavelength ($dT/d\lambda$) was plotted as a function of photon energy ($h\nu$), and the band gap was extracted from the position of the maximum derivative peak corresponding to the absorption edge (Figure 6) [54].The optical band gap energy (Eg) values of the ZnO thin films synthesized at different precursor concentrations are presented in Table 3.

Table 2: Band gap energy of ZnO thin films prepared at different precursor concentrations.

Precursor concentration (M)	Band gap energy (eV)
0.05	3.25
0.10	3.19
0.15	3.18
0.20	3.20
0.25	3.22
0.30	3.21

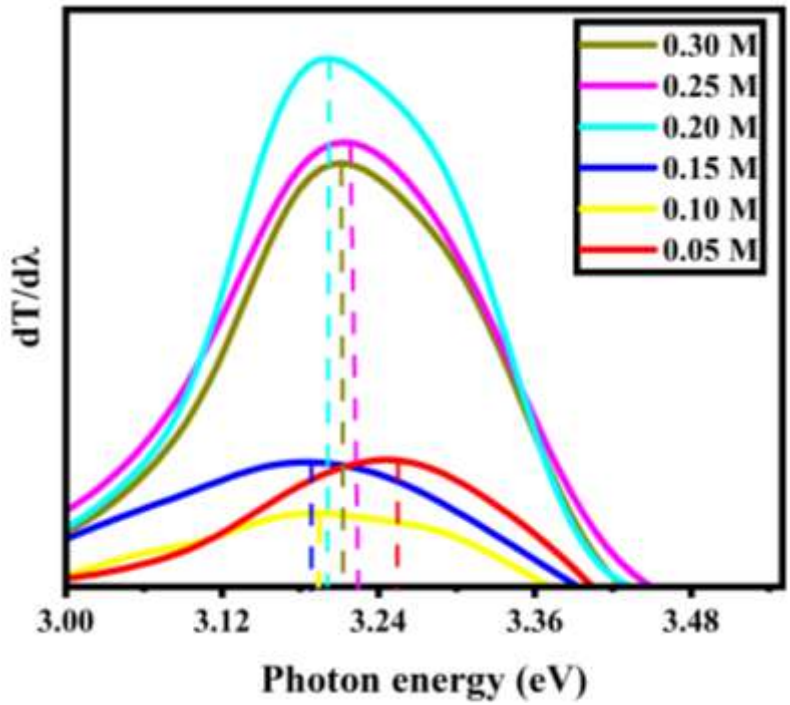

Figure 6: dT/dλ curve as a function of photon energy for ZnO thin films prepared at different precursor concentrations.

The optical band gap energy values of the synthesized ZnO thin films range between 3.18 eV and 3.25 eV and are in good agreement with those reported by Abdulrahman et al. [27]. The obtained values are slightly lower than that of bulk ZnO, which can be attributed to the presence of intrinsic defects such as oxygen vacancies, zinc interstitials, and other structural imperfections [4]. These defects introduce localized states within the band gap, thereby modifying the optical transition energies. The observed variation in the optical band gap is strongly correlated with the structural evolution of the films induced by precursor concentration. As the concentration increases from 0.05 M to 0.15 M, a decrease in the band gap energy from 3.25 eV to 3.18 eV is observed. This reduction can be mainly associated with the increase in crystallite size, as confirmed by XRD analysis, which reduces the quantum confinement-like effects and modifies the electronic structure of the material [37]. In addition, this regime corresponds to a decrease in dislocation density and microstrain, indicating a relaxation of structural defects. Since dislocations and strain-induced distortions create localized energy levels within the band gap, their reduction leads to a modification of the density of states and hence influences the optical absorption edge. Moreover, increasing precursor concentration can also induce internal mechanical stress within the thin films due to lattice mismatch and differences in thermal expansion coefficients between the film and the substrate [55]. These stresses further perturb the band structure, contributing to the observed narrowing of the band gap. At higher concentrations (0.20 M to 0.30 M), a slight increase in the band gap is observed. This behavior is attributed to improved crystallinity, accompanied by a reduction in crystallite size and a more ordered lattice structure. The decrease in structural disorder and defect density at these concentrations leads to a partial restoration of the band structure, resulting in a slight widening of the optical band gap.

Photoluminescence Properties:-

The photoluminescence properties of ZnO thin films were investigated using photoluminescence (PL) spectroscopy. Figure 7 presents the PL spectra of the samples prepared at different precursor concentrations. The photoluminescence properties of ZnO thin films were investigated using PL spectroscopy. Figure 7 presents the PL spectra of the samples prepared at different precursor concentrations. Three emission peaks are observed, centered at approximately 390 nm (3.18 eV), 446 nm (2.78 eV), and 490 nm (2.53 eV), respectively. The dominant peak at 390 nm is attributed to free exciton recombination corresponding to 3.18 eV (390 nm), associated with the direct wide band gap transition in ZnO thin films at room temperature [56]**.** The presence of emission peaks in the visible region around 446 nm (2.78 eV) and 490 nm (2.53 eV), located in the blue and blue-green spectral regions, indicates the existence of intrinsic defects within the ZnO lattice [57]. According to contemporary defect models, these deep-level

emissions are commonly associated with zinc interstitials (Zni) and oxygen vacancies (V_o) [58]. The blue emission centered at 446 nm is predominantly associated with Zni-related shallow donor states [59], whereas the blue-green emission around 490 nm is mainly attributed to oxygen-vacancy (V_o)-related defect levels located within the band gap [57]**.** Therefore, the visible luminescence observed in the present study is likely governed by the combined contribution of Zn_i and V_o defects [57]**.** In this regard, the thin films synthesized at a precursor concentration of 0.05 M exhibit a strong emission intensity in the visible region, indicating a higher defect density in these samples. In contrast, ZnO thin films prepared at a concentration of 0.25 M show a significantly lower visible emission intensity. These films therefore contain fewer structural defects and exhibit improved crystalline quality.

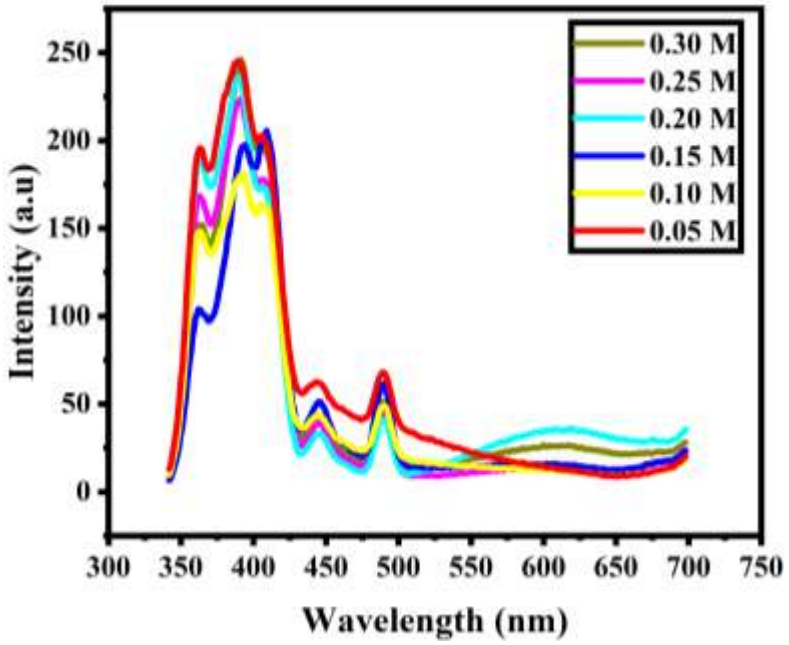

Figure 7: Photoluminescence spectra of ZnO thin films prepared at different precursor concentrations.

Conclusion:-

ZnO thin films were synthesized using a two-step process. The first step consisted of the deposition of a ZnO seed layer by the spin-coating technique from a 0.01 M solution prepared by dissolving 0.044 g of zinc acetate dihydrate (precursor) in 20 mL of ethanol (solvent). This seed layer acts as a nucleation platform for the growth of nanostructures. The second step involved the growth of ZnO thin films by chemical bath deposition on the previously prepared seed layers, with the precursor concentration varied from 0.05 M to 0.30 M in increments of 0.05 M. The growth solution was an equimolar mixture of aqueous solutions of zinc nitrate hexahydrate and hexamethylenetetramine. The obtained ZnO thin films were subsequently annealed at 400 °C for 3 hours to improve crystallinity. The synthesized films were characterized using X-ray diffraction, UV-Visible spectroscopy, and photoluminescence spectroscopy to investigate their structural and optical properties, as well as the presence of defects.

The results clearly demonstrate the influence of precursor concentration on the physical properties of ZnO thin films. X-ray diffraction analysis revealed that all synthesized ZnO films are polycrystalline and crystallize in the hexagonal wurtzite structure, with a preferential orientation along the (002) plane as the precursor concentration increases. Weak crystallinity is observed at 0.05 M, while the increasing intensity of the (002) peak with concentration indicates improved crystallinity. UV-Visible spectroscopy results show that all ZnO thin films are highly transparent, with transmittance exceeding 80 %. The optical band gap of the films varies between 3.18 eV and 3.25 eV. Photoluminescence spectra exhibit three emission peaks centered at approximately 390 nm (3.18 eV), 446 nm (2.78 eV), and 490 nm (2.53 eV), corresponding to near-band-edge emission and defect-related emissions. Overall, a precursor concentration of 0.25 M appears to be optimal, providing a good balance between high crystallinity, high optical transparency, and reduced defect density.

Acknowledgements:-
The authors would like to sincerely thank CERME (Togo) for its financial support and Alagappa Government Arts College, Karaikudi (India), for providing the facilities for the formal analyses.

References:-
[1]S. Aydemir, S. Karakaya, Effects of withdrawal speed on the structural and optical properties of sol–gel derived ZnO thin films, J. Magn. Magn. Mater. 373 (2015) 33–39. https://doi.org/10.1016/j.jmmm.2014.01.077.
[2]H. Yin, V.A. Coleman, P.S. Casey, B. Angel, H.J. Catchpoole, L. Waddington, M.J. McCall, A comparative study of the physical and chemical properties of nano-sized ZnO particles from multiple batches of three commercial products, J. Nanoparticle Res. 17 (2015) 96. https://doi.org/10.1007/s11051-014-2851-y.
[3]M. Soylu, M. Coskun, Controlling the properties of ZnO thin films by varying precursor concentration, J. Alloys Compd. 741 (2018) 957–968. https://doi.org/10.1016/j.jallcom.2018.01.079.
[4]S.G. Ruvalcaba-Manzo, R. Ramírez-Bon, R. Ochoa-Landín, S.J. Castillo, A Comprehensive Study of the Optical, Structural, and Morphological Properties of Chemically Deposited ZnO Thin Films, Inorganics 13 (2025) 331. https://doi.org/10.3390/inorganics13100331.
[5]Z. Zang, X. Zeng, J. Du, M. Wang, X. Tang, Femtosecond laser direct writing of microholes on roughened ZnO for output power enhancement of InGaN light-emitting diodes, Opt. Lett. 41 (2016) 3463. https://doi.org/10.1364/OL.41.003463.
[6]N. Jalali, J. Briscoe, Y.Z. Tan, P. Woolliams, M. Stewart, P.M. Weaver, M.G. Cain, S. Dunn, ZnO nanorod surface modification with PDDA/PSS Bi-layer assembly for performance improvement of ZnO piezoelectric energy harvesting devices, J. Sol-Gel Sci. Technol. 73 (2015) 544–549. https://doi.org/10.1007/s10971-014-3512-4.
[7]Rajesh Kumar, Girish Kumar, O. Al-Dossary, Ahmad Umar, ZnO nanostructured thin films: Depositions, properties and applications—A review, Mater. Express 5 (2015). https://doi.org/doi:10.1166/mex.2015.1204.
[8]J.Y. Park, D.E. Song, S.S. Kim, An approach to fabricating chemical sensors based on ZnO nanorod arrays, Nanotechnology 19 (2008) 105503. https://doi.org/10.1088/0957-4484/19/10/105503.
[9]B. Khodadadi, M. Bordbar, A. Yeganeh-Faal, Optical, structural, and photocatalytic properties of Cd-doped ZnO powders prepared via sol–gel method, J. Sol-Gel Sci. Technol. 77 (2016) 521–527. https://doi.org/10.1007/s10971-015-3877-z.
[10]M. Thambidurai, N. Muthukumarasamy, D. Velauthapillai, C. Lee, Chemical bath deposition of ZnO nanorods for dye sensitized solar cell applications, J. Mater. Sci. Mater. Electron. 24 (2013) 1921–1926. https://doi.org/10.1007/s10854-012-1035-8.
[11]Z. Yin, N. Chen, R. Dai, L. Liu, X. Zhang, X. Wang, J. Wu, C. Chai, On the formation of well-aligned ZnO nanowall networks by catalyst-free thermal evaporation method, J. Cryst. Growth 305 (2007) 296–301. https://doi.org/10.1016/j.jcrysgro.2007.04.043.
[12]J. Husna, M.M. Aliyu, M.A. Islam, P. Chelvanathan, N.R. Hamzah, M.S. Hossain, M.R. Karim, N. Amin, Influence of Annealing Temperature on the Properties of ZnO Thin Films Grown by Sputtering, Energy Procedia 25 (2012) 55–61. https://doi.org/10.1016/j.egypro.2012.07.008.
[13]J.P. Labis, M. Hezam, A. Al-Anazi, H. Al-Brithen, A.A. Ansari, A. Mohamed El-Toni, R. Enriquez, G. Jacopin, M. Al-Hoshan, Pulsed laser deposition growth of 3D ZnO nanowall network in nest-like structures by two-step approach, Sol. Energy Mater. Sol. Cells 143 (2015) 539–545. https://doi.org/10.1016/j.solmat.2015.07.045.
[14]M. Opel, S. Geprägs, M. Althammer, T. Brenninger, R. Gross, Laser molecular beam epitaxy of ZnO thin films and heterostructures, J. Phys. Appl. Phys. 47 (2014) 034002. https://doi.org/10.1088/0022-3727/47/3/034002.
[15]B. Wu, S.-W. Zhuang, C. Chi, Z.-F. Shi, J.-Y. Jiang, X. Dong, W.-C. Li, Y.-T. Zhang, B.-L. Zhang, G.-T. Du, The growth of ZnO on stainless steel foils by MOCVD and its application in light emitting devices, Phys. Chem. Chem. Phys. 18 (2016) 5614–5621. https://doi.org/10.1039/C5CP06826F.
[16]U. Pal, P. Santiago, Controlling the Morphology of ZnO Nanostructures in a Low-Temperature Hydrothermal Process, J. Phys. Chem. B 109 (2005) 15317–15321. https://doi.org/10.1021/jp052496i.
[17]O. Ako, M. Baneto, A.D. Gboglo, M. Senthilkumar, M. Haris, Temperature-controlled growth of ZnO Thin films by spray pyrolysis: Influence on physical properties for photovoltaic applications, Edelweiss Appl. Sci. Technol. 9 (2025) 1052–1066. https://doi.org/10.55214/2576-8484.v9i10.10594.
[18]O. Baka, A. Azizi, S. Velumani, G. Schmerber, A. Dinia, Effect of Al concentrations on the electrodeposition and properties of transparent Al-doped ZnO thin films, J. Mater. Sci. Mater. Electron. 25 (2014) 1761–1769. https://doi.org/10.1007/s10854-014-1796-3.
[19]F.E. Ghodsi, H. Absalan, Comparative Study of ZnO Thin Films Prepared by Different Sol-Gel Route, Acta Phys. Pol. A 118 (2010) 659–664. https://doi.org/10.12693/APhysPolA.118.659.

[20]M. Baneto, D. Djagbai, E. Mouzou, A.D. Gboglo, O. Ako, M.F. Kouide, D. Kassegne, Controlled Deposition of Zn Thin Films by Spin Coating: Influence of Spin Speed on Film Microstructure and Transparency, J. Nano-Electron. Phys. 17 (2025) 05016-1-05016–8. https://doi.org/10.21272/jnep.17(5).05016.
[21]A.D. Gboglo, M. Baneto, O. Ako, K.S. Gadedjisso-Tossou, B. Grandidier, M. Haris, M. Senthilkumar, K. N'Konou, Structural, morphological and optical properties of ZnO thin films grown by time-dependent chemical bath deposition, Int. J. Renew. Energy Dev. 15 (2026) 66–75. https://doi.org/10.61435/ijred.2026.61665.
[22]A.F. Abdulrahman, S.M. Ahmed, N.M. Ahmed, M.A. Almessiere, Enhancement of ZnO Nanorods Properties Using Modified Chemical Bath Deposition Method: Effect of Precursor Concentration, Crystals 10 (2020) 386. https://doi.org/10.3390/cryst10050386.
[23]G. Jia, Y. Wang, J. Yao, Growth mechanism of Zno nano-structure using chemical bath deposition, 6 (2010) 303–307.
[24]A.F. Abdulrahman, S.M. Ahmed, S.M. Hamad, A.A. Barzinjy, Effect of Growth Temperature on Morphological, Structural, and Optical Properties of ZnO Nanorods Using Modified Chemical Bath Deposition Method, J. Electron. Mater. 50 (2021) 1482–1495. https://doi.org/10.1007/s11664-020-08705-7.
[25]K. Mosalagae, D.M. Murape, L.M. Lepodise, Effects of growth conditions on properties of CBD synthesized ZnO nanorods grown on ultrasonic spray pyrolysis deposited ZnO seed layers, Heliyon 6 (2020) e04458. https://doi.org/10.1016/j.heliyon.2020.e04458.
[26]Alphonse Déssoudji Gboglo, Mazabalo Baneto, Ognanmi Ako, Muthiah Haris, Muthusamy Senthilkuma, Role of hexamethylenetetramine/zinc nitrate hexahydrate molar ratio in controlling structural, morphological and optical properties of ZnO thin films synthesized by CBD, (2025). https://doi.org/10.3934/matersci.2025039.
[27]A.F. Abdulrahman, S.M. Ahmed, N.M. Ahmed, M.A. Almessiere, Enhancement of ZnO Nanorods Properties Using Modified Chemical Bath Deposition Method: Effect of Precursor Concentration, Crystals 10 (2020) 386. https://doi.org/10.3390/cryst10050386.
[28]G. Syrrokostas, K. Govatsi, S.N. Yannopoulos, High-Quality, Reproducible ZnO Nanowire Arrays Obtained by a Multiparameter Optimization of Chemical Bath Deposition Growth, Cryst. Growth Des. 16 (2016) 2140–2150. https://doi.org/10.1021/acs.cgd.5b01812.
[29]A.D. Gboglo, M. Baneto, K.S. Gadedjisso-Tossou, O. Ako, A.C. Ahyi, M. Haris, M. Senthilkumar, K. N'konou, B. Grandidier, K. Beltako, K.A. Amou, M.M. Dzagli, Co-Effect of pH Control Agent and pH Value on the Physical Properties of ZnO Thin Films Obtained by Chemical Bath Deposition for Potential Application in Dye-Sensitized Solar Cells, Surfaces 8 (2025) 46. https://doi.org/10.3390/surfaces8030046.
[30]S. Paul, A. Das, M. Palit, S. Bhunia, A. Karmakar, S. Chattopadhyay, Investigation Of The Properties Of Single-step and Double-step Grown ZnO Nanowires Using Chemical Bath Deposition Technique, Adv. Mater. Lett. 7 (2016) 610–615. https://doi.org/10.5185/amlett.2016.6298.
[31]G. Jia, Y. Wang, J. Yao, Growth mechnism of ZnO nano-structure using chemical bath deposition, 6 (2010).
[32]S. Kurtaran, Al doped ZnO thin films obtained by spray pyrolysis technique: Influence of different annealing time, Opt. Mater. (2021). https://doi.org/https://doi.org/10.1016/j.optmat.2021.110908.
[33]H.F. McMurdie, M.C. Morris, E.H. Evans, B. Paretzkin, W. Wong-Ng, L. Ettlinger, Standard X-Ray Diffraction Powder Patterns from The JCPDS Research Associateship, 1 (1986) 40. https://doi.org/https://doi.org/10.1017/S0885715600011593.
[34]A.A. Abuelsamen, S. Mahmud, A. Seeni, N.H.M. Kaus, O.F. Farhat, Effects of precursor concentrations on the optical and morphological properties of ZnO nanorods on glass substrate for UV photodetector, Superlattices Microstruct. 111 (2017) 536–545. https://doi.org/10.1016/j.spmi.2017.07.007.
[35]Y. Kumar, Controlling of ZnO nanostructures by solute concentration and its effect on growth, structural and optical properties, (2015). https://doi.org/http://iopscience.iop.org/2053-1591/2/10/105017.
[36]C.-H. Chao, C.-H. Chan, J.-J. Huang, L.-S. Chang, H.-C. Shih, Manipulated the band gap of 1D ZnO nano-rods array with controlled solution concentration and its application for DSSCs, Curr. Appl. Phys. 11 (2011) S136–S139. https://doi.org/10.1016/j.cap.2010.11.056.
[37]O. Ako, M. Baneto, M. Senthilkumar, M. Haris, A.D. Gboglo, K.S. Gadedjisso-Tossou, A.C. Ahyi, K. Beltako, K.A. Amou, Simultaneous effect of precursor sources and concentration on structural, morphological and optical properties of ZnO nanostructured thin films for photovoltaic applications, Int. J. Renew. Energy Dev. 14 (2025) 495–504. https://doi.org/10.61435/ijred.2025.61069.
[38]M. Thambidurai, N. Muthukumarasamy, D. Velauthapillai, C. Lee, Chemical bath deposition of ZnO nanorods for dye sensitized solar cell applications, J. Mater. Sci. Mater. Electron. 24 (2013) 1921–1926. https://doi.org/10.1007/s10854-012-1035-8.
[39]R. Mohamed, M.S.A. Anuar, Structural and Electrochemical Behaviors of ZnO Structure: Effect of Different Zinc Precursor Molarity, Condens. Matter 7 (2022) 71. https://doi.org/10.3390/condmat7040071.

[40]R. Romero, D. Leinen, E.A. Dalchiele, J.R. Ramos-Barrado, F. Martín, The effects of zinc acetate and zinc chloride precursors on the preferred crystalline orientation of ZnO and Al-doped ZnO thin films obtained by spray pyrolysis, Thin Solid Films 515 (2006) 1942–1949. https://doi.org/10.1016/j.tsf.2006.07.152.
[41]O. Lupan, T. Pauporté, L. Chow, B. Viana, F. Pellé, L.K. Ono, B. Roldan Cuenya, H. Heinrich, Effects of annealing on properties of ZnO thin films prepared by electrochemical deposition in chloride medium, Appl. Surf. Sci. 256 (2010) 1895–1907. https://doi.org/10.1016/j.apsusc.2009.10.032.
[42]K. Thongsuriwong, P. Amornpitoksuk, S. Suwanboon, Structure, morphology, photocatalytic and antibacterial activities of ZnO thin films prepared by sol–gel dip-coating method, Adv. Powder Technol. 24 (2013) 275–280. https://doi.org/10.1016/j.apt.2012.07.002.
[43]T. Amakali, Likius.S. Daniel, V. Uahengo, N.Y. Dzade, N.H. De Leeuw, Structural and Optical Properties of ZnO Thin Films Prepared by Molecular Precursor and Sol–Gel Methods, Crystals 10 (2020) 132. https://doi.org/10.3390/cryst10020132.
[44]S. Mustapha, M.M. Ndamitso, A.S. Abdulkareem, J.O. Tijani, D.T. Shuaib, A.K. Mohammed, A. Sumaila, Comparative study of crystallite size using Williamson-Hall and Debye-Scherrer plots for ZnO nanoparticles, Adv. Nat. Sci. Nanosci. Nanotechnol. 10 (2019) 045013. https://doi.org/10.1088/2043-6254/ab52f7.
[45]K.R. Devi, G. Selvan, M. Karunakaran, G.R. Kanna, S. Maheswari, Role of solution concentration on zno thin films prepared by silar method, (2016). hal-05461982.
[46]V. Mote, Y. Purushotham, B. Dole, Williamson-Hall analysis in estimation of lattice strain in nanometer-sized ZnO particles, J. Theor. Appl. Phys. 6 (2012) 6. https://doi.org/10.1186/2251-7235-6-6.
[47]G.C.A.M. Janssen, Stress and strain in polycrystalline thin films, Thin Solid Films 515 (2007) 6654–6664. https://doi.org/10.1016/j.tsf.2007.03.007.
[48]M. Huff, Review Paper: Residual Stresses in Deposited Thin-Film Material Layers for Micro- and Nano-Systems Manufacturing, Micromachines 13 (2022) 2084. https://doi.org/10.3390/mi13122084.
[49]A.F. Abdulrahman, S.M. Ahmed, S.M. Hamad, M.A. Almessiere, N.M. Ahmed, S.M. Sajadi, Effect of different pH values on growth solutions for the ZnO nanostructures, Chin. J. Phys. 71 (2021) 175–189. https://doi.org/10.1016/j.cjph.2021.02.013.
[50]M. Bakry, W. Ismail, M. Abdelfatah, A. El-Shaer, Low-cost fabrication methods of ZnO nanorods and their physical and photoelectrochemical properties for optoelectronic applications, Sci. Rep. 14 (2024) 23788. https://doi.org/10.1038/s41598-024-73352-5.
[51]M. Baneto, A. Enesca, Y. Lare, K. Jondo, K. Napo, A. Duta, Effect of precursor concentration on structural, morphological and opto-electric properties of ZnO thin films prepared by spray pyrolysis, Ceram. Int. 40 (2014) 8397–8404. https://doi.org/10.1016/j.ceramint.2014.01.048.
[52]E.Ş. Tüzemen, S. Eker, H. Kavak, R. Esen, Dependence of film thickness on the structural and optical properties of ZnO thin films, Appl. Surf. Sci. 255 (2009) 6195–6200. https://doi.org/10.1016/j.apsusc.2009.01.078.
[53]T. Amakali, Likius.S. Daniel, V. Uahengo, N.Y. Dzade, N.H. De Leeuw, Structural and Optical Properties of ZnO Thin Films Prepared by Molecular Precursor and Sol–Gel Methods, Crystals 10 (2020) 132. https://doi.org/10.3390/cryst10020132.
[54]A.D. Gboglo, M. Baneto, O. Ako, A.-R. Ali-Tagba, B. Grandidier, K. N'konou, Combined Influence of Precursor Source and Solvent Type on Microstructural and Optical Properties of Spin-Coated ZnO Thin Films, Surfaces 9 (2026) 50. https://doi.org/10.3390/surfaces9020050.
[55]Y. Rama Denny Muchtar, T. Firmansyah, A. Trenggono, D. Wijaya, G. Antarnusa, A. Suherman, Effect of Precursor Concentration and Annealed Substrate Temperature on the Crystal Structure, Electronic and Optical Properties of ZnO thin film, J. Pure Appl. Chem. Res. 9 (2020) 57–65. https://doi.org/10.21776/ub.jpacr.2020.009.01.514.
[56]A.-S. Gadallah, M.M. El-Nahass, Structural, Optical Constants and Photoluminescence of ZnO Thin Films Grown by Sol-Gel Spin Coating, Adv. Condens. Matter Phys. 2013 (2013) 1–11. https://doi.org/10.1155/2013/234546.
[57]S. Hullavarad, N. Hullavarad, D. Look, B. Claflin, Persistent Photoconductivity Studies in Nanostructured ZnO UV Sensors, Nanoscale Res. Lett. 4 (2009) 1421. https://doi.org/10.1007/s11671-009-9414-7.
[58]A. Galdámez-Martinez, G. Santana, F. Güell, P.R. Martínez-Alanis, A. Dutt, Photoluminescence of ZnO Nanowires: A Review, Nanomaterials 10 (2020) 857. https://doi.org/10.3390/nano10050857.
[59]J. Lv, C. Li, Z. Chai, Defect luminescence and its mediated physical properties in ZnO, J. Lumin. 208 (2019) 225–237. https://doi.org/10.1016/j.jlumin.2018.12.050.